PBH formation due to critical collapse during the QCD epoch

Sobrinho J. L. G., Jesus P. D. F., Cunha J. N.[1]

August 2025

Grupo de Astronomia da Universidade da Madeira
Faculdade de Ciências Exatas e da Engenharia
Universidade da Madeira, Campus da Penteada, 9020-105 Funchal
astro@uma.pt
https://astro.web.uma.pt/Grupo/index.htm

Abstract

Primordial Black Holes (PBHs) might have formed in the early Universe as a consequence of the collapse of density fluctuations with amplitude δ above some threshold δ_c. The mass of a PBH is generally expected to be on the order of the horizon mass at its formation epoch. However, this may not hold true when $\delta \gtrsim \delta_c$. In these cases, the phenomenon of critical collapse must be considered, which results in a much broader mass spectrum for the PBH population. We explored PBH formation during the QCD epoch for a Crossover Model (CM) within the regime of critical collapse. As a general result, we found that although the number of PBHs is of the same order of magnitude for analogous cases, their mass spectrum is considerably broader in the case of critical collapse, spanning across four or more orders of magnitude toward the smaller masses.

Keywords: black hole physics - stars: black holes - cosmology: cosmological parameters, dark energy, dark matter, early Universe, phase transition, inflation - particle physics: standard model

[1]Jesus P. D. F. and Cunha J. N. were supported, respectively, by the programmes **INGRESSA 2025** and **Estágios de Verão 2025** both promoted by the **Secretaria Regional da Educação**, through the **Direção Regional de Juventude** (DRJ) - Região Autónoma da Madeira.

1 Introduction

Primordial black holes (PBHs) may have formed in the early Universe due to the collapse of density fluctuations (e.g. Hawking, 1971; Carr, 1975; Novikov et al., 1979). During inflation, fluctuations of quantum origin are stretched to scales much larger than the cosmological horizon, becoming causally disconnected from physical processes. The inflationary era is then followed by a radiation-dominated epoch during which these fluctuations can re-enter the cosmological horizon. For a given physical scale k, the **horizon crossing time** t_k (i.e., the instant when that scale re-enters the cosmological horizon) is given by (e.g. Blais et al., 2003):

$$ck = a(t_k)H(t_k), \tag{1}$$

where $a(t_k)$ is the scale factor and $H(t_k)$ the Hubble parameter (cf. Sobrinho, 2011; Sobrinho et al., 2016). The collapse that gives rise to the formation of a PBH is now possible, but only if the amplitude of the density fluctuation at horizon crossing:

$$\delta_k = \frac{\Delta m}{m}, \tag{2}$$

is larger than a specific **threshold** value δ_c. If $\delta_k \geq \delta_c$, then the expansion of the overdense region will, eventually, come to a halt, followed by its collapse leading to the formation of a PBH. On the other hand, if $\delta_k < \delta_c$, then the fluctuation dissipates without forming a PBH.

Numerically solving the relativistic hydrodynamical equations for a radiation-dominated Universe, it is possible to show that $0.4 \leq \delta_c \leq 0.6$, with the true value being a function of the shape of the energy density perturbation. Here we consider $\delta_c \approx 0.50$, which corresponds to the typical Mexican-Hat perturbation profile (e.g. Musco et al., 2021; Musco, Jedamzik, & Young, 2024).

The threshold δ_c is constant through the radiation-dominated epoch, the exception occurring during cosmological phase transitions, when the value of δ_c decreases (as a consequence of the decrease of the sound speed). This is relevant, since a lower value of δ_c favours PBH formation (e.g. Carr, 2003). The Standard Model of Particle Physics (SMPP) predicts two such phase transitions:

- **Electroweak (EW) phase transition** at temperatures of ~ 100 GeV (when the age of the Universe was $\sim 10^{-10}$ s), responsible for the spontaneous breaking of the EW symmetry. PBHs formed during this epoch would have $\sim 10^{-6}\ M_\odot$ (cf. Sobrinho, 2011).

- **Quantum Chromodynamics (QCD) phase transition** at $T_c \approx$ 170 MeV when quarks and gluons became confined in hadrons. PBHs formed during this epoch would have $\sim 0.5\ M_\odot$ (cf. Sobrinho, 2011; Sobrinho & Augusto, 2020).

Less dramatic reductions in the value of δ_c may also occur during cosmic annihilation epochs such as the e^+e^- annihilation (EPA) epoch, favouring the formation of intermediate mass PBHs (e.g. Sobrinho & Augusto, 2024).

The majority of the PBHs formed at a particular epoch would have masses within the order of the horizon mass, M_H, at that epoch (e.g. Carr, 2003):

$$M_{PBH}(t_k) = M_H(t_k), \tag{3}$$

where (e.g. Carr, 2003):

$$M_H(t) \sim 10^{15} \left(\frac{t}{10^{-23}\ \mathrm{s}} \right)\ \mathrm{g}. \tag{4}$$

However, in the case of density perturbations with δ only slightly larger than δ_c we may have to consider the phenomenon of critical collapse in which case the PBH masses rather obey the scaling law (Niemeyer & Jedamzik, 1999):

$$M_{PBH}(t_k) = K M_H(t_k) \left(\delta - \delta_c\right)^\gamma, \tag{5}$$

where K is a dimensionless constant and the critical exponent $\gamma \approx 0.36$ is universal (e.g. Sobrinho & Augusto, 2007; Kuhnel, Rampf, & Sandstad, 2015). This scaling law has been found to hold down to $(\delta - \delta_c) \sim 10^{-10}$ (Musco & Miller, 2013). We will distinguish between these two situations by referring to them as **simple collapse** (equation 3) and **critical collapse** (equation 5).

The aim of this report is to study the effect of gravitational collapse on PBH formation during the QCD epoch. The report is organized as follows: after reviewing, in Section 2, we give some key general results up to the PBH density parameter and the PBH number density and show how these are affected when critical collapse is taken into account. In Section 3 we consider PBH formation during the QCD epoch for different scenarios. Finally, in Section 4 we present some conclusions and ideas for future work.

2 The PBH density parameter

The probability that a fluctuation crossing the horizon at some instant t_k has of collapsing and forming a PBH can be written as (e.g. Niemeyer &

Jedamzik, 1998):

$$P(\delta, t_k) = \frac{1}{\sqrt{2\pi}\sigma(t_k)} \exp\left(-\frac{\delta^2}{2\sigma^2(t_k)}\right), \tag{6}$$

where it is assumed that the primordial density fluctuations obey a Gaussian distribution, with $\sigma^2(t_k)$ being the mass variance at horizon crossing. The mass variance can be written as (e.g. Sobrinho & Augusto, 2020):

$$\sigma^2(k) = \int_0^{\frac{k_e}{k}} x^3 \delta_H^2(k_c) \frac{P(kx)}{P(k_c)} W_{TH}^2(x) W_{TH}^2(\frac{x}{\sqrt{3}}) dx, \tag{7}$$

where $k_e \approx 0.01$ m^{-1} is the smallest scale generated by inflation, the function W_{TH} represents the Fourier transform of the top-hat window function, $\delta_H^2(k_c)$ is the amplitude of the density perturbation normalized to the pivot scale $k_c = 0.05$ Mpc$^{-1} \approx 1.6 \times 10^{-24}$ m^{-1}, with $\delta_H^2(k_c) \approx 2.198 \times 10^{-9}$ (cf. Planck Collaboration et al., 2016) and P is the power spectrum of the density fluctuations, which, for a running-tilt power-law spectrum, can be written as (e.g. Sobrinho & Augusto, 2020):

$$P(k) = P(k_c) \left(\frac{k}{k_c}\right)^{n(k)-1}. \tag{8}$$

The function $n(k)$ appearing in equation (8), which specifies the dependence of the power spectrum on the comoving wavenumber k, is called the spectral index (e.g. Carr, Kühnel, & Sandstad, 2016):

$$n(k) = n_0 + \sum_{i \geq 1} \frac{n_i}{(i+1)!} \left(\ln \frac{k}{k_c}\right)^i, \tag{9}$$

where n_0, n_1 and n_2 represent, respectively, the spectral index at the pivot scale k_c, the running of the spectral index and the running of the running of the spectral index (e.g. Erfani, 2014). In order for a non-negligible amount of PBHs to be produced, we must have a blue spectrum, i.e., we must have $n(k) > 1$ at least during some epochs in the early Universe (e.g. Blais et al., 2003).

Known values are $n(k_c) = n_0 \approx 0.9476$, $n_1 = 0.001$ and $n_2 = 0.022$ (e.g. Erfani, 2014). In order to obtain a blue spectrum in some relevant epochs during radiation domination, Sobrinho & Augusto (2020) worked on the plane (n_3, n_4) assuming $n_i = 0$ when $i \geq 5$. In that case, we may consider (cf. Sobrinho & Augusto, 2020):

$$n(k) = n_0 + \frac{n_1}{2} \ln \frac{k}{k_c} + \frac{n_2}{6} \left(\ln \frac{k}{k_c}\right)^2 + \frac{n_3}{24} \left(\ln \frac{k}{k_c}\right)^3 + \frac{n_4}{120} \left(\ln \frac{k}{k_c}\right)^4. \tag{10}$$

We are interested in situations for which $n(k)$ shows a local **maximum** at some point $k = k_{max}$ with $n_{max} = n(k_{max}) > 1$. In order to obtain that, we consider (cf. Sobrinho & Augusto, 2020):

$$n_{max} = n_0 + \frac{n_1}{2} \ln \frac{k_{max}}{k_c} + \frac{n_2}{6} \left(\ln \frac{k_{max}}{k_c} \right)^2 + \frac{n_3}{24} \left(\ln \frac{k_{max}}{k_c} \right)^3 + \frac{n_4}{120} \left(\ln \frac{k_{max}}{k_c} \right)^4, \tag{11}$$

$$\frac{dn(k)}{dk} \mid_{k=k_{max}} = 0 \Leftrightarrow \frac{n_1}{2} + \frac{n_2}{3} \ln \frac{k_{max}}{k_c} + \frac{n_3}{8} \left(\ln \frac{k_{max}}{k_c} \right)^2 + \frac{n_4}{30} \left(\ln \frac{k_{max}}{k_c} \right)^3 = 0. \tag{12}$$

Given a pair of values (n_{max}, k_{max}), or equivalently $(n_{max}, t_{k_{max}})$, we can determine the corresponding pair of values (n_3, n_4) (cf. Sobrinho & Augusto, 2020):

$$n_3 = \frac{-4 \left(24n_0 - 24n_{max} + 9n_1 \ln \frac{k_{max}}{k_c} + 2n_2 \left(\ln \frac{k_{max}}{k_c} \right)^2 \right)}{\left(\ln \frac{k_{max}}{k_c} \right)^3}, \tag{13}$$

$$n_4 = \frac{20 \left(18n_0 - 18n_{max} + 6n_1 \ln \frac{k_{max}}{k_c} + n_2 \left(\ln \frac{k_{max}}{k_c} \right)^2 \right)}{\left(\ln \frac{k_{max}}{k_c} \right)^4}. \tag{14}$$

Considering, for example, $n_{max} = 1.803$ (clearly a blue spectrum) and $t_{k_{max}} = 10^{-3}$ s we get from equations (13) and (14) $n_3 = 0.0099$ and $n_4 = -0.0033$. With this set of values, we have plotted the curve $n(k)$ (see Figure 1).

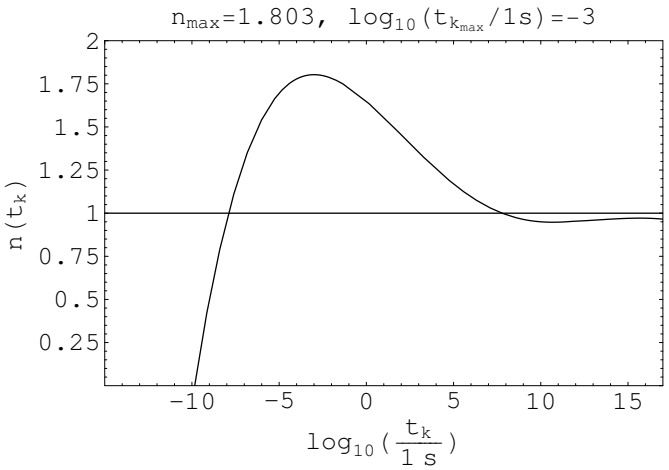

Figure 1: The curve $n(t_k)$ (equation 10) when $n_{max} = 1.803$ and $t_{k_{max}} = 10^{-3}$ s.

The PBH density parameter evaluated at the horizon crossing is given by (e.g. Niemeyer & Jedamzik, 1998):

$$\Omega_{PBH}(t_k) = \frac{1}{M_H(t_k)} \int_{\delta_c}^{+\infty} M_{PBH}(\delta, t_k) P(\delta, t_k) d\delta. \tag{15}$$

If we neglect the effect of critical collapse as given by equation (5), then we must consider instead simple collapse (equation 3) which can be assumed valid as a first approach. Inserting equations (3) and (6) into equation (15) we get:

$$\beta(t_k) = \frac{1}{\sqrt{2\pi}\sigma(t_k)} \int_{\delta_c}^{+\infty} \exp\left(-\frac{\delta^2}{2\sigma^2(t_k)}\right) d\delta. \tag{16}$$

When assuming that all the PBHs formed due to the gravitational collapse of density fluctuations that crossed the horizon at the instant t_k will form with the mass $M_H(t_k)$ (cf. equation 4) it is common to refer to Ω_{PBH} as β. This expression gives the fraction of the Universe that is converted into PBHs at the instant t_k. More exactly, it is the fraction of the Universe converted in PBHs due to the gravitational collapse of density fluctuations that crossed the horizon at the instant t_k.

If we want to consider the effect of the scaling law (cf. equation 5), then the expression for $\beta(t_k)$ as given by equation (16) is no longer useful. In that case, we must consider instead:

$$\Omega_{PBH}(t_k) = \frac{1}{\sqrt{2\pi} M_H(t_k)\sigma(t_k)} \int_{\delta_c}^{+\infty} M_{PBH}(\delta, t_k) \exp\left(-\frac{\delta^2}{2\sigma^2(t_k)}\right) d\delta, \tag{17}$$

which was obtained by inserting equation (6) into equation (15). Equation (17) gives the PBH density parameter at the instant t_k including PBHs of all masses. In order to get the present-day value of $\Omega_{PBH}(t_k)$, we must take into account the redshift (e.g. Ricotti, Ostriker, & Mack, 2008):

$$\Omega_{PBH}(t_0, t_k)\,[1 + z(t_{eq})] = [1 + z(t_k)]\,\Omega_{PBH}(t_k), \tag{18}$$

where $t_{eq} \approx 2.37 \times 10^{12}$ s is the age of the Universe at matter-radiation equality (cf. Sobrinho et al., 2016). Taking into account the relation between redshift and scale factor, we may also write equation (18) in the form (e.g. Sobrinho & Augusto, 2020):

$$\Omega_{PBH}(t_0, t_k) = \frac{a(t_{eq})}{a(t_k)}\Omega_{PBH}(t_k). \tag{19}$$

The present-day number density of PBHs formed at a given epoch t_k, assuming simple collapse (i.e., all the PBHs formed with the horizon mass - cf. equations 3 and 4), can be written as (e.g. Sobrinho, 2011; Sobrinho & Augusto, 2020):

$$n_{\rm PBH}(t_0, t_k) = \rho_{\rm c}(t_0)\frac{\Omega_{\rm PBH}(t_0, t_k)}{M_H(t_k)}, \tag{20}$$

where $\rho_{\rm c}(t_0) \approx 8.26 \times 10^{-27}$ kg m^{-3} is the critical density of the Universe at the present time (e.g. Sobrinho & Augusto, 2020). If we are interested on the present-day value of the PBH number density due to PBHs exclusively formed between two given instants, t_{k_1} and t_{k_2}, then we may consider (cf. Sobrinho & Augusto, 2020):

$$n_{\rm PBH}(t_0) = \rho_c(t_0)\int_{t_{k_1}}^{t_{k_2}} \frac{\Omega_{\rm PBH}(t_0, t_k)}{M_H(t_k)}{\rm d}t_k, \tag{21}$$

with $t_{k_1} \gtrsim 10^{-23}$ s, since PBHs eventually formed before that epoch have already evaporated (e.g. Sobrinho & Augusto, 2014), and $t_{k_2} \lesssim 10^5$ s, since PBHs formed at that epoch and later on would have $\gtrsim 10^{10}$ $M_\odot$ and we are not aware of any black hole candidates with masses above that value (e.g. Saglia et al., 2016).

If we want to consider the effect of critical collapse in the population of PBHs, then we must replace $M_{PBH}(\delta, t_k)$ in equation (17) by the expression given by equation (5). In order to do that, we consider the substitution on the variable under the sign of integration from δ to M_{PBH}. From equation (5) we get:

$$\delta = \left(\frac{M_{PBH}(t_k)}{K M_H(t_k)}\right)^{1/\gamma} + \delta_c(t_k). \tag{22}$$

Differentiating equation (22) with respect to M_{PBH} we obtain:

$$\frac{d\delta}{dM_{PBH}(t_k)} = \frac{1}{K\gamma M_H(t_k)} \left(\frac{M_{PBH}(t_k)}{KM_H(t_k)} \right)^{\frac{1-\gamma}{\gamma}}. \tag{23}$$

When $\delta = \delta_c$ we get $M_{PBH} = 0$ and when $\delta \to +\infty$ it turns out that $M_{PBH} \to +\infty$. Inserting all this into equation (17) and rearranging the terms, we get:

$$\Omega_{PBH}(t_k) = \frac{1}{\sqrt{2\pi}\gamma K^{1/\gamma} M_H(t_k)^{\frac{1+\gamma}{\gamma}} \sigma(t_k)} \times$$

$$\int_0^{+\infty} M_{PBH}(t_k)^{1/\gamma} \exp\left(-\frac{\left(\left(\frac{M_{PBH}(t_k)}{KM_H(t_k)} \right)^{1/\gamma} + \delta_c(t_k) \right)^2}{2\sigma^2(t_k)} \right) dM_{PBH}. \tag{24}$$

This gives us the fraction due to PBHs of all masses formed after the collapse of density fluctuations that crossed the horizon at the instant t_k. If we are interested on the value of Ω_{PBH} due to PBHs within a specific mass range, say, $M_{PBH_1} \leq M_{PBH} \leq M_{PBH_2}$, we may consider:

$$\Omega_{PBH}(t_k, M_{PBH_1}, M_{PBH_2}) = \frac{1}{\sqrt{2\pi}\gamma K^{1/\gamma} M_H(t_k)^{\frac{1+\gamma}{\gamma}} \sigma(t_k)} \times$$

$$\int_{M_{PBH_1}}^{M_{PBH_2}} M_{PBH}(t_k)^{1/\gamma} \exp\left(-\frac{\left(\left(\frac{M_{PBH}(t_k)}{KM_H(t_k)} \right)^{1/\gamma} + \delta_c(t_k) \right)^2}{2\sigma^2(t_k)} \right) dM_{PBH}. \tag{25}$$

Similarly, if we want the value of Ω_{PBH} due to PBHs with masses within the range $M_{PBH_1} \leq M_{PBH} \leq M_{PBH_2}$ that were formed after density fluctuations that crossed the horizon within the epoch $t_{k_1} \leq t_k \leq t_{k_2}$, then we may write:

$$\Omega_{PBH}(t_{k_1}, t_{k_2}, M_{PBH_1}, M_{PBH_2}) = \frac{1}{\sqrt{2\pi}\gamma K^{1/\gamma}} \times$$

$$\int_{t_{k_1}}^{t_{k_2}} \int_{M_{PBH_1}}^{M_{PBH_2}} \frac{1}{M_H(t_k)^{\frac{1+\gamma}{\gamma}} \sigma(t_k)} M_{PBH}(t_k)^{1/\gamma} \times \tag{26}$$

$$\exp\left(-\frac{\left(\left(\frac{M_{PBH}(t_k)}{K M_H(t_k)} \right)^{1/\gamma} + \delta_c(t_k) \right)^2}{2\sigma^2(t_k)} \right) dM_{PBH} dt_k.$$

Assuming that $t_{k_2} - t_{k_1} \gtrsim 0$ we may write, after equation (19):

$$\Omega_{PBH}(t_0, t_{k_1}, t_{k_2}, M_{PBH_1}, M_{PBH_2}) \approx \frac{a(t_{eq})}{a(t_{k_m})} \Omega_{PBH}(t_{k_1}, t_{k_2}, M_{PBH_1}, M_{PBH_2}), \tag{27}$$

where we are considering the average:

$$t_{k_m} = \frac{t_{k_1} + t_{k_2}}{2}. \tag{28}$$

Assuming that besides $t_{k_2} - t_{k_1} \gtrsim 0$ we also have $M_{PBH_2} - M_{PBH_1} \gtrsim 0$ then we may write after equation (21):

$$n_{PBH}(t_0, t_{k_1}, t_{k_2}, M_{PBH_1}, M_{PBH_2}) = \frac{\rho_c(t_0) \Omega_{PBH}(t_0, t_{k_1}, t_{k_2}, M_{PBH_1}, M_{PBH_2})}{M_{PBH_m}}, \tag{29}$$

where we are considering the average:

$$M_{PBH_m} = \frac{M_{PBH_1} + M_{PBH_2}}{2}. \tag{30}$$

Equation (29) gives us the present-day PBH number density for PBHs with masses within the range $[M_{PBH_1}, M_{PBH_2}]$ formed after density fluctuations that crossed the horizon at the epoch $[t_{k_1}, t_{k_2}]$. In order to obtain the number of PBHs inside a given volume V, we write (assuming that PBHs are distributed homogeneously):

$$N_{PBH}(t_0, t_{k_1}, t_{k_2}, M_{PBH_1}, M_{PBH_2}) = n_{PBH}(t_0, t_{k_1}, t_{k_2}, M_{PBH_1}, M_{PBH_2}) V. \tag{31}$$

3 PBHs formed during the QCD phase transition epoch

We now consider the effect of critical collapse on the formation of PBHs during the QCD epoch. Following Sobrinho & Augusto (2020) we consider for the QCD three different models: Crossover Model (CM), Lattice fit Model (LM) and Bag Model (BM). We will pursue with the study of the five selected cases, namely, $t_{k_{max}} = 10^{-1}$ s, $t_{k_{max}} = 10^{-3}$ s, $t_{k_{max}} = 10^{-5}$ s, $t_{k_{max}} = 10^{-7}$ s, and $t_{k_{max}} = 10^{-9}$ s. We will start with the $\beta(t_k)$ curves (cf. equation 16) from Sobrinho & Augusto (2020) with two updates that might introduce some slight changes:

- the background value of the threshold is now $\delta_c = 0.5$ instead of $\delta_c = 0.43$: this directly affects the curve for $\delta_c(t_k)$ during the QCD epoch;
- the observational constraints on PBHs were also updated (c.f. Carr et al., 2021a; Jesus & Sobrinho, 2025): this affects the values of n_{max}.

In Figure 2 we show the updated $\beta(t_k)$ curve for the case $t_{k_{max}} = 10^{-1}$ s with $n_{max} = 1.948$ which is valid for all the three QCD models.

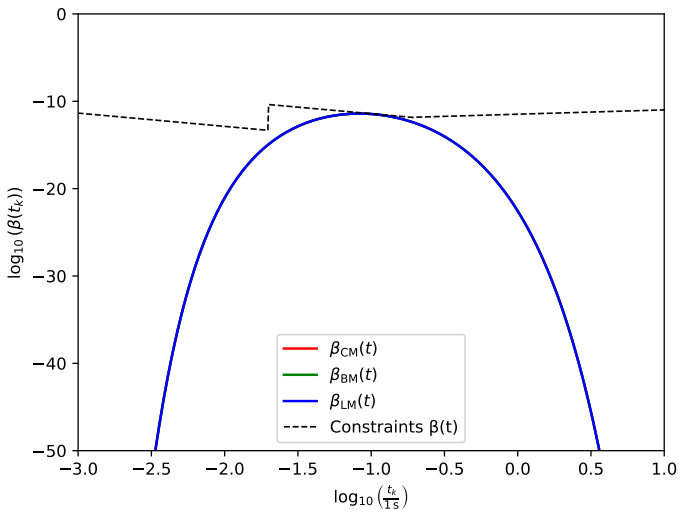

Figure 2: The curve $\beta(t_k)$ when $t_{k_{max}} = 10^{-1}$ s and $n_{max} = 1.948$ (cf. equation 16). The curve is valid for all the three QCD models (CM, LM and BM).

In Figure 3 we show the $\beta(t_k)$ curves (cf. equation 16) for the case $t_{k_{max}} = 10^{-3}$ s with $n_{max} = 1.808$ (CM), $n_{max} = 1.793$ (LM) and $n_{max} = 1.776$ (BM).

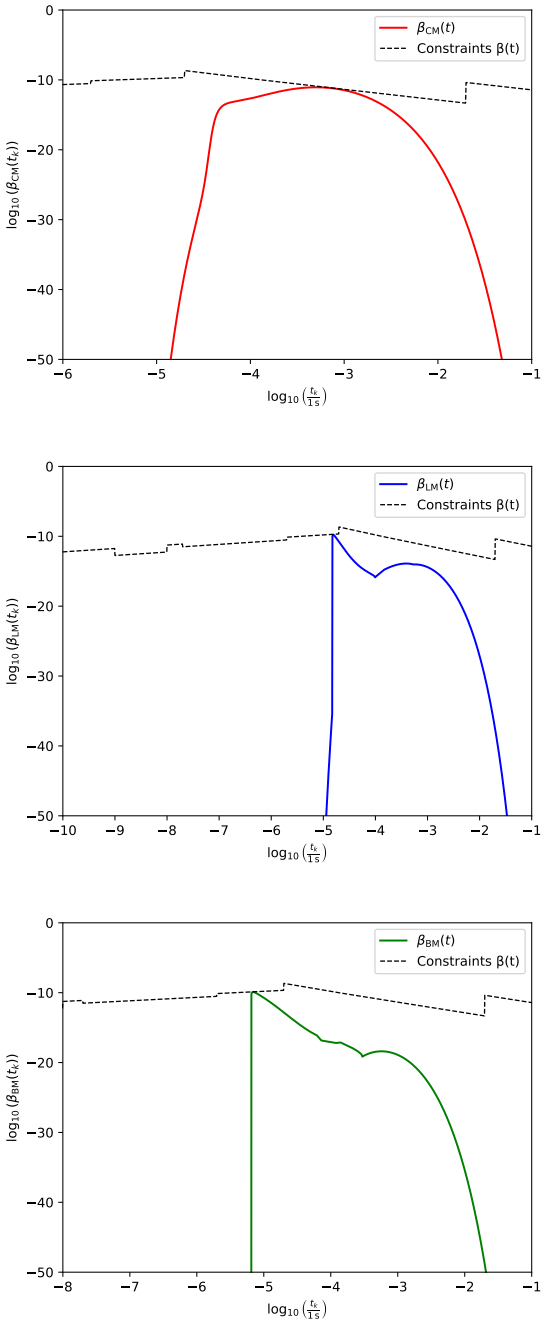

Figure 3: The curve $\beta(t_k)$ (cf. equation 16) when $t_{k_{max}} = 10^{-3}$ s with $n_{max} = 1.808$ (CM), $n_{max} = 1.793$ (LM) and $n_{max} = 1.776$ (BM).

In Figure 4 we show the $\beta(t_k)$ curves for the case $t_{k_{max}} = 10^{-5}$ s with $n_{max} = 1.708$ (CM), $n_{max} = 1.617$ (LM) and $n_{max} = 1.554$ (BM).

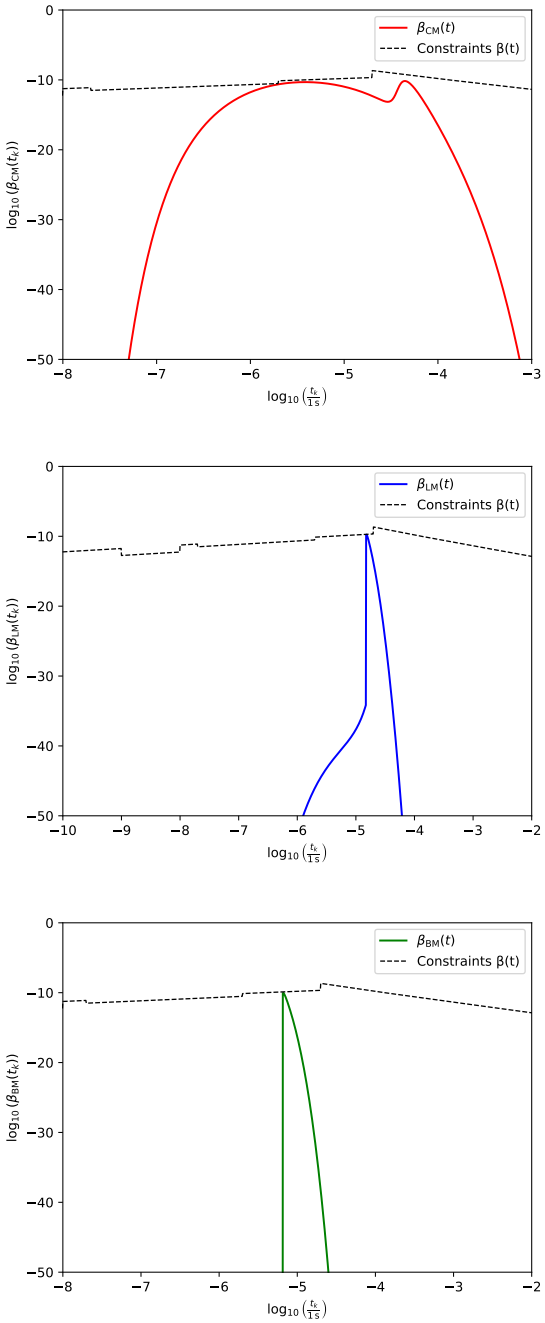

Figure 4: The curve $\beta(t_k)$ (cf. equation 16) when $t_{k_{max}} = 10^{-5}$ s with $n_{max} = 1.708$ (CM), $n_{max} = 1.617$ (LM) and $n_{max} = 1.554$ (BM).

In Figure 5 we show the $\beta(t_k)$ curves for the case $t_{k_{max}} = 10^{-7}$ s with $n_{max} = 1.619$ (CM), $n_{max} = 1.618$ (LM) and $n_{max} = 1.552$ (BM).

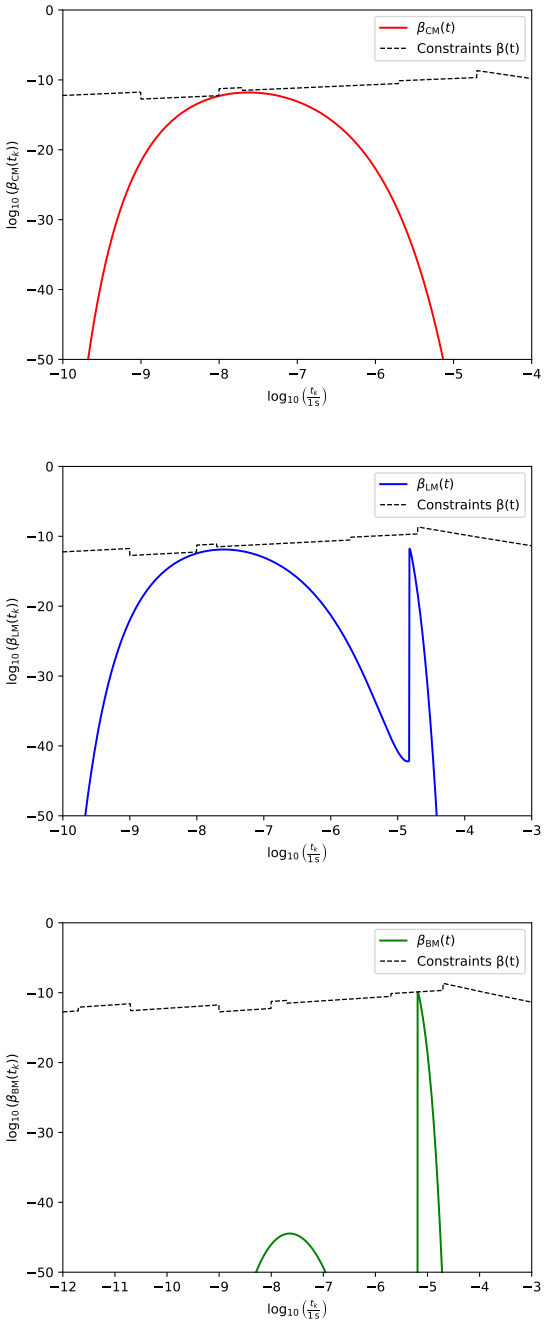

Figure 5: The curve $\beta(t_k)$ (cf. equation 16) when $t_{k_{max}} = 10^{-7}$ s with $n_{max} = 1.619$ (CM), $n_{max} = 1.618$ (LM) and $n_{max} = 1.552$ (BM).

Finally, in Figure 6 we show the $\beta(t_k)$ curves for the case $t_{k_{max}} = 10^{-9}$ s with $n_{max} = 1.552$ for all the three QCD models.

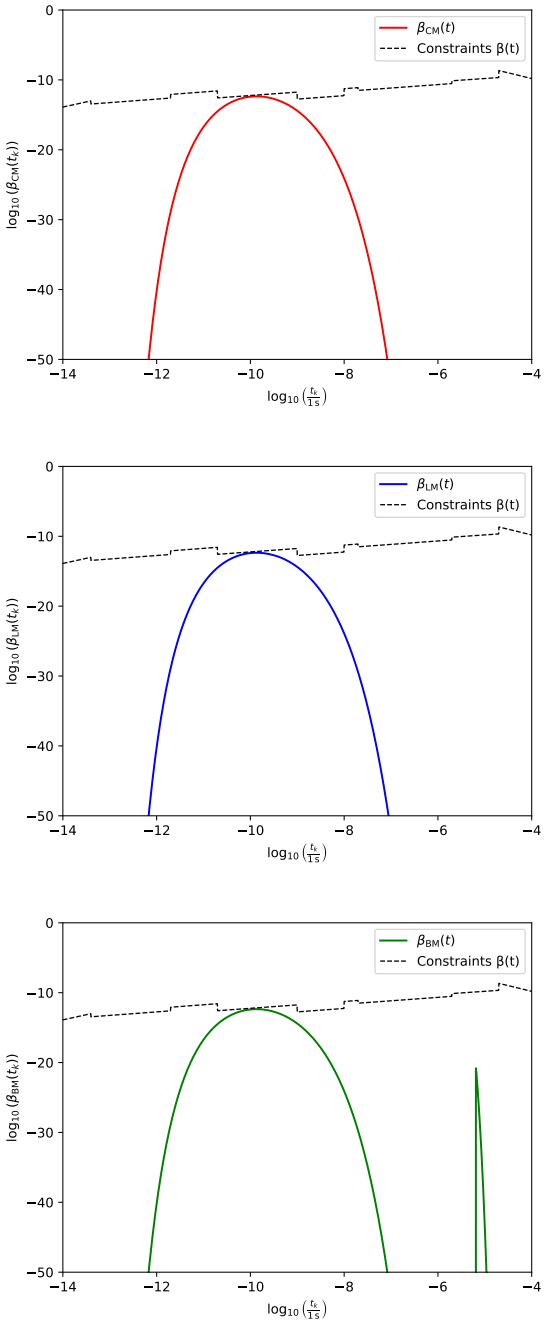

Figure 6: The curve $\beta(t_k)$ (cf. equation 16) when $t_{k_{max}} = 10^{-9}$ s with $n_{max} = 1.552$ for all the three QCD models (CM, LM and BM).

When $t_{k_{max}} = 10^{-1}$ s the effect of the QCD is quite negligible. In that case, we just considered in equation (26) the background value of the PBH

formation threshold (i.e., $\delta_c(t_k) = 0.5$). For the other values of $t_{k_{max}}$, we are working with, the values of $\delta_c(t_k)$ are obtained following the same procedure as explained in Sobrinho et al. (2016). In the case of a QCD CM it turns out that $\delta_c(t_k)$ is a single-valued function, meaning that we could just replace the corresponding values in equation (26). However, when addressing the QCD BM or LM this is not always the case since a new window for PBH formation emerges at some point (cf. Sobrinho et al., 2016), implying that it would be necessary to split the integral in equation (26) into the sum of two integrals.

We now consider PBH formation during the QCD epoch for a CM within the critical collapse regime. For each of the five selected cases ($t_{k_{max}} = 10^{-1}$ s, $t_{k_{max}} = 10^{-3}$ s, $t_{k_{max}} = 10^{-5}$ s, $t_{k_{max}} = 10^{-7}$ s, and $t_{k_{max}} = 10^{-9}$ s) we divided the plane $(\log(t_k), \log(M_{PBH}))$ into sufficiently small $\Delta\log(t_k) \times \Delta\log(M_{PBH})$ cells (we chose to work with $\Delta\log(t_k) = 0.005$ and $\Delta\log(M_{PBH}) = 0.005$ since with these values the results already converge reasonably). For each cell we determined the corresponding value of $\Omega_{PBH}(t_0, t_{k_1}, t_{k_2}, M_{PBH_1}, M_{PBH_2})$ with the help of equations (26) and (27). Applying equation (29) we determined for each cell the corresponding number density of PBHs in the present-day Universe and, with the help of equation (31) the effective number of PBHs (N_{PBH}) per Gpc^3. This procedure allowed us to determine the region on the $(\log(t_k), \log(M_{PBH}))$ plane which is relevant for the case under study (i.e., the region for which each cell contains at least one PBH per Gpc^3).

For example, when $t_{k_{max}} = 10^{-1}$ s and $n_{max} = 1.948$ we find that the relevant region is completely enclosed within the limits $-5 < \log\left(\frac{t_k}{1\text{ s}}\right) < 1$ and $-10 < \log\left(\frac{M_{PBH}}{1\ M_\odot}\right) < 8$. Dividing this particular region into cells with sides $\Delta\log(t_k) = 0.005$ and $\Delta\log(M_{PBH}) = 0.005$ we get a total of $1200 \times 3600 = 4\,320\,000$ cells. We elaborate two matrices with these dimensions, one for Ω_{PBH}, which we call A_Ω, and another one for N_{PBH}, which we call A_N.

Given the matrix A_Ω and a specific value of M_{PBH} we can integrate with respect to t_k in order to obtain $\Omega_{PBH}(t_0, M_{PBH})$, i.e., the contribution to Ω_{PBH} due to PBHs with mass M_{PBH}, within the critical collapse regime, regardless of the epoch in which they were formed. For comparison purposes, we can also think about the $\Omega_{PBH}(t_0, M_{PBH})$ curve associated with the simple collapse regime. This curve is obtained by applying equation (19) to each value of $\beta(t_k)$ from Figure 2 (in the case $t_{k_{max}} = 10^{-1}$ s).

Similarly, given the matrix A_N and a specific value of M_{PBH} we can integrate with respect to t_k in order to obtain $n_{PBH}(t_0, M_{PBH})$ (cf. equation 29), i.e., the contribution to the PBH number density due to PBHs with mass M_{PBH}, within the critical collapse regime, regardless of the epoch in which

they were formed. Multiplying the obtained values by a chosen volume V (which we will take as 1 Gpc^3) we obtain the number of PBHs with mass M_{PBH} within that volume (cf. equation 31).

In Figures 7 and 8 we show the curves $\Omega_{PBH}(t_0, M_{PBH})$ and $N_{PBH}(t_0, M_{PBH})$, respectively, for the simple and critical collapse regime when $t_{k_{max}} = 10^{-1}$ s and $n_{max} = 1.948$.

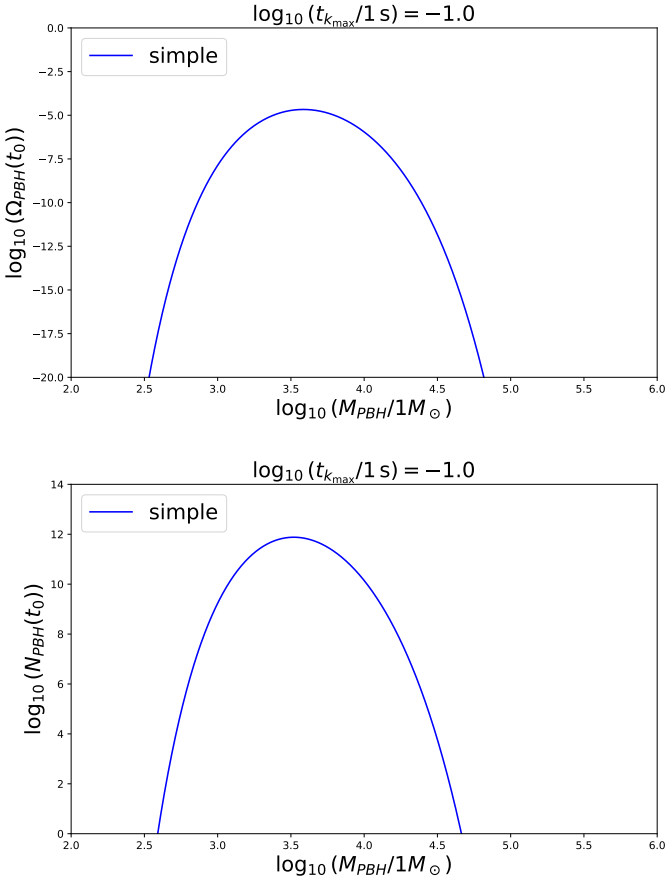

Figure 7: The curves $\Omega_{PBH}(t_0, M_{PBH})$ (top) and $N_{PBH}(t_0, M_{PBH})$ (bellow) for simple collapse regime when $t_{k_{max}} = 10^{-1}$ s (see text for more details).

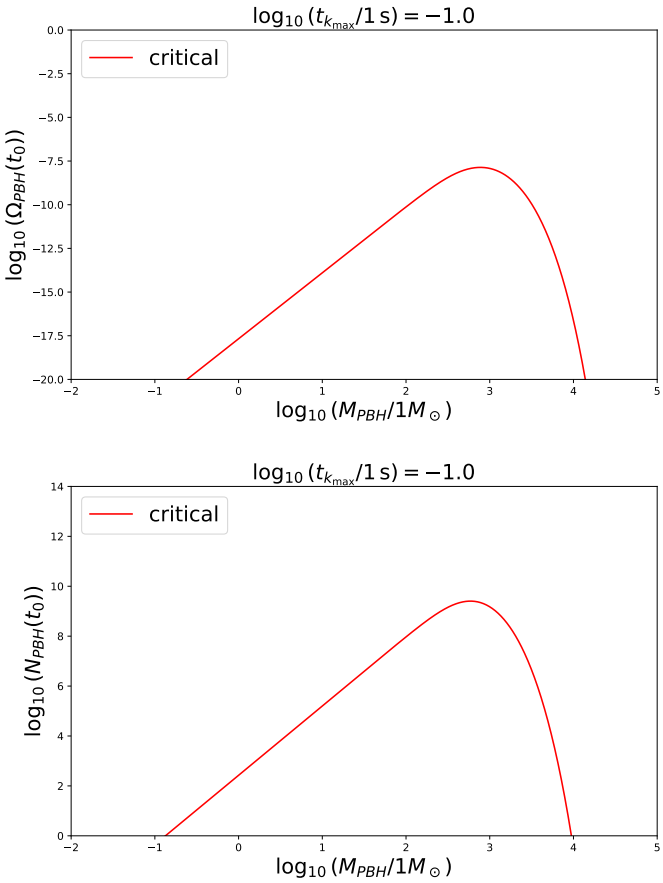

Figure 8: The curves $\Omega_{PBH}(t_0, M_{PBH})$ (top) and $N_{PBH}(t_0, M_{PBH})$ (bellow) for the critical collapse regime when $t_{k_{max}} = 10^{-1}$ s (see text for more details).

To obtain the curves for the simple collapse regime, we use equations (16) and (19) to determine the points of $\Omega_{PBH}(t_0, t_k)$, for each t_k, and then, after using equation (20), we multiply by the volume of 1 Gpc^3 and get the points of $N_{PBH}(t_0, t_k)$. For the critical collapse regime, the curves are obtained through the matrices A_Ω and A_N. For each interval $\Delta \log(M_{PBH})$ we sum all cells in the t_k axis, for both matrices, and obtain the points to plot $\Omega_{PBH}(t_0, t_k)$ and $N_{PBH}(t_0, t_k)$, respectively.

We follow the same procedure in order to obtain the $\Omega_{PBH}(t_0, M_{PBH})$ and $N_{PBH}(t_0, M_{PBH})$ curves for the QCD CM for the cases $t_{k_{max}} = 10^{-3}$ s (Figures 9 and 10), $t_{k_{max}} = 10^{-5}$ s (Figures 11 and 12), $t_{k_{max}} = 10^{-7}$ s (Figures 13 and 14) and $t_{k_{max}} = 10^{-9}$ s (Figures 15 and 16).

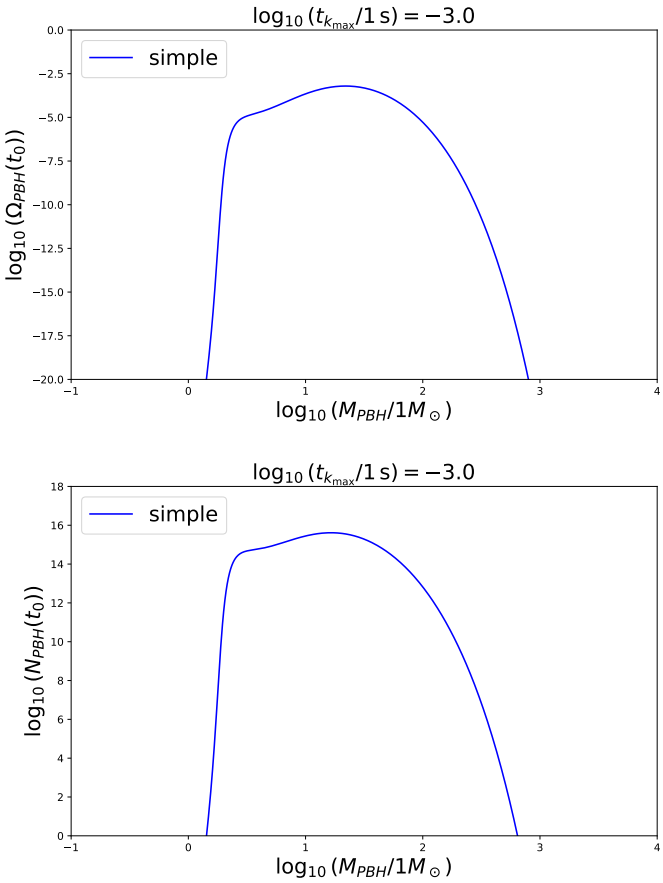

Figure 9: The curves $\Omega_{PBH}(t_0, M_{PBH})$ (top) and $N_{PBH}(t_0, M_{PBH})$ (bellow) for simple collapse regime when $t_{k_{max}} = 10^{-3}$ s (see text for more details).

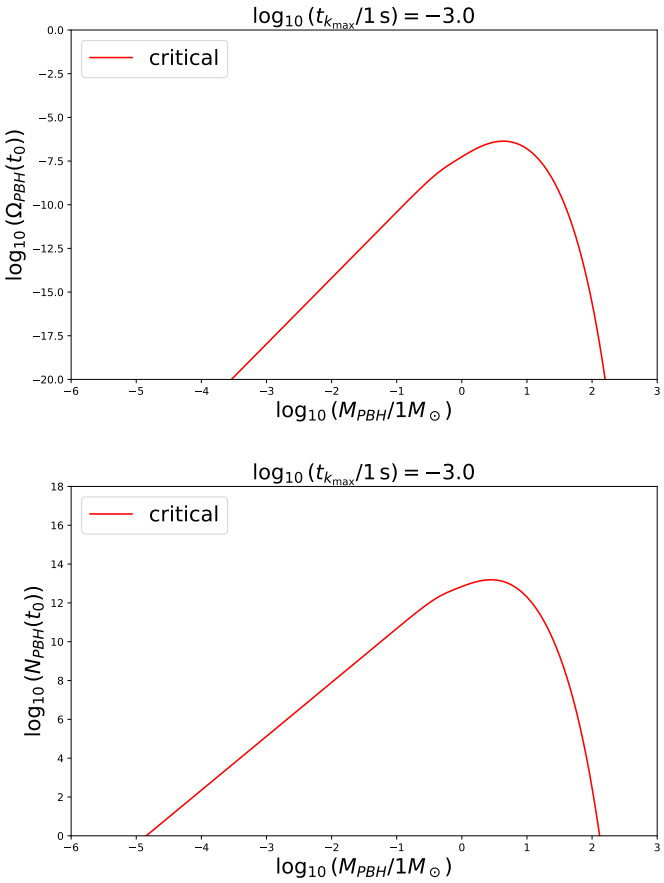

Figure 10: The curves $\Omega_{PBH}(t_0, M_{PBH})$ (top) and $N_{PBH}(t_0, M_{PBH})$ (bellow) for the critical collapse regime when $t_{k_{max}} = 10^{-3}$ s (see text for more details).

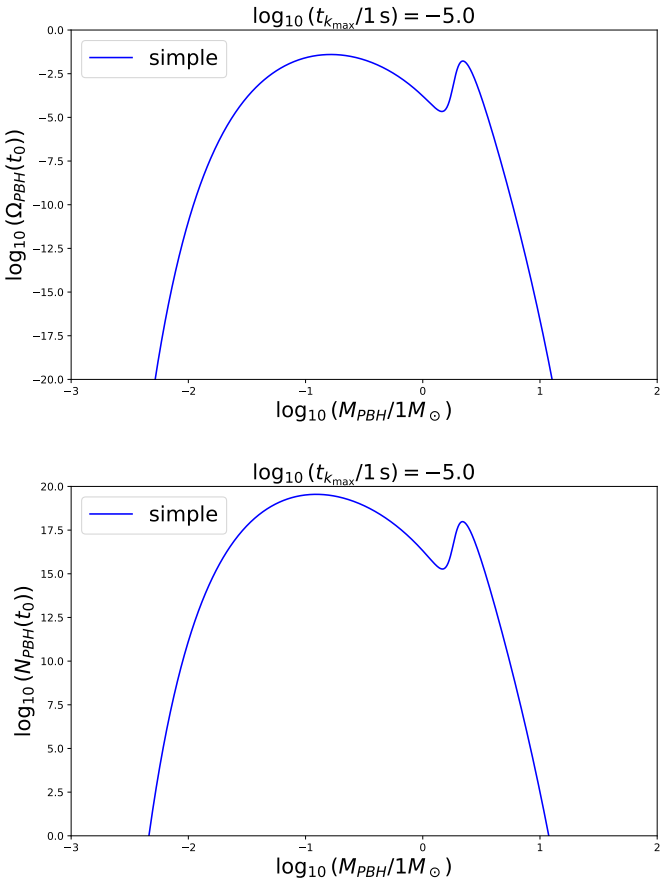

Figure 11: The curves $\Omega_{PBH}(t_0, M_{PBH})$ (top) and $N_{PBH}(t_0, M_{PBH})$ (bellow) for simple collapse regime when $t_{k_{max}} = 10^{-5}$ s (see text for more details).

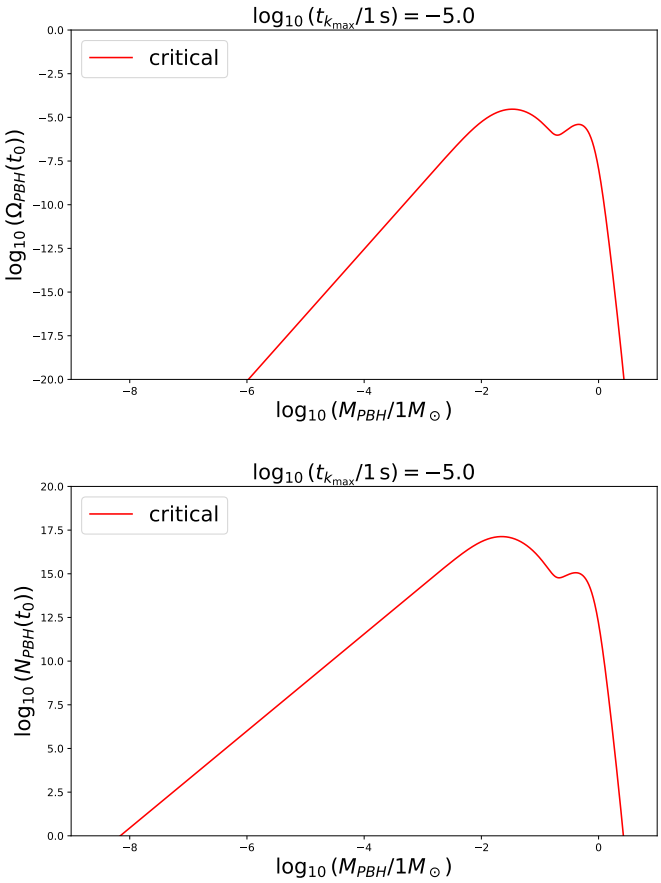

Figure 12: The curves $\Omega_{PBH}(t_0, M_{PBH})$ (top) and $N_{PBH}(t_0, M_{PBH})$ (bellow) for the critical collapse regime when $t_{k_{max}} = 10^{-5}$ s (see text for more details).

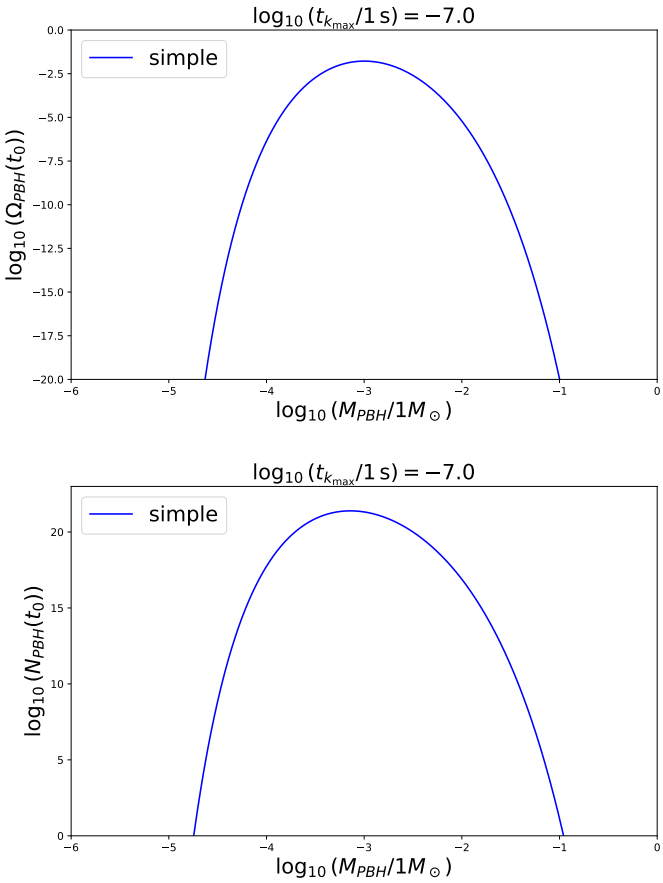

Figure 13: The curves $\Omega_{PBH}(t_0, M_{PBH})$ (top) and $N_{PBH}(t_0, M_{PBH})$ (bellow) for simple collapse regime when $t_{k_{max}} = 10^{-7}$ s (see text for more details).

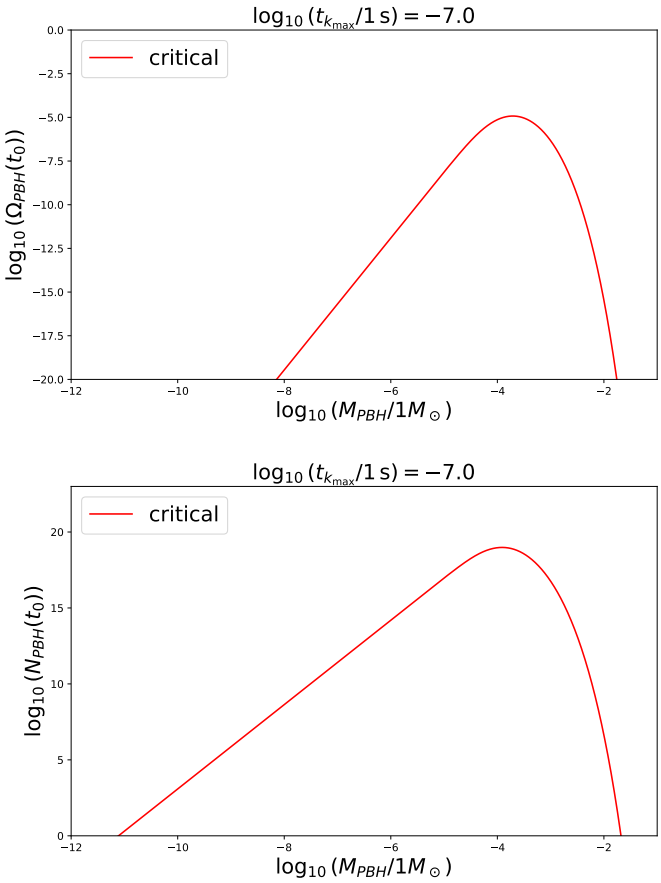

Figure 14: The curves $\Omega_{PBH}(t_0, M_{PBH})$ (top) and $N_{PBH}(t_0, M_{PBH})$ (bellow) for the critical collapse regime when $t_{k_{max}} = 10^{-7}$ s (see text for more details).

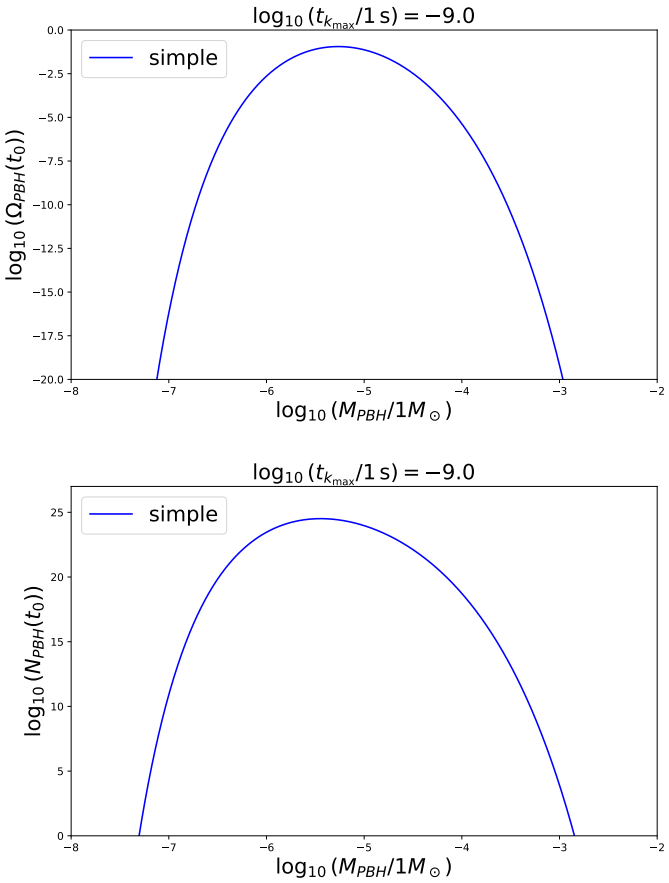

Figure 15: The curves $\Omega_{PBH}(t_0, M_{PBH})$ (top) and $N_{PBH}(t_0, M_{PBH})$ (bellow) for simple collapse regime when $t_{k_{max}} = 10^{-9}$ s (see text for more details).

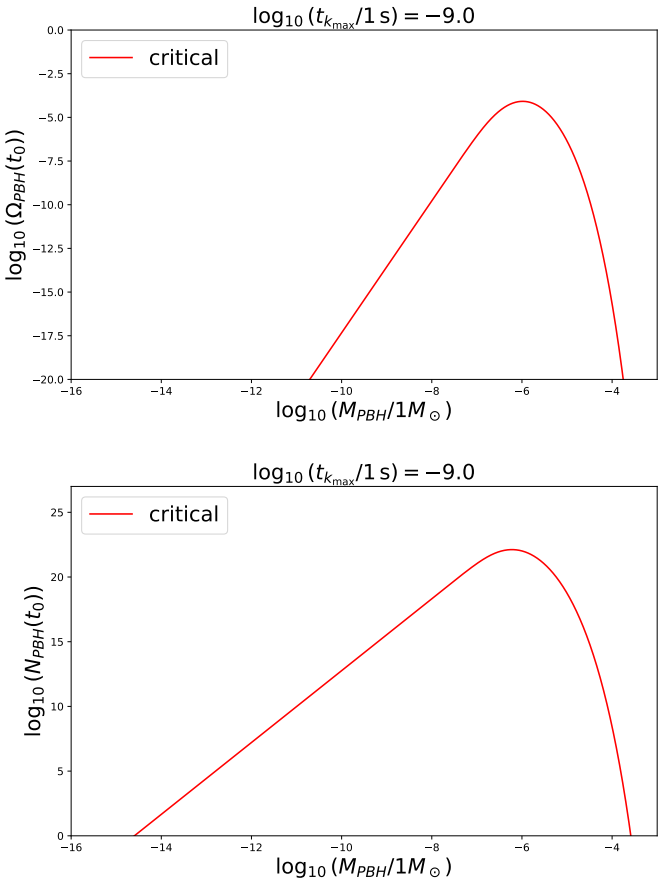

Figure 16: The curves $\Omega_{PBH}(t_0, M_{PBH})$ (top) and $N_{PBH}(t_0, M_{PBH})$ (bellow) for the critical collapse regime when $t_{k_{max}} = 10^{-9}$ s (see text for more details).

The global value of the PBH density parameter, Ω_{PBH}, for a given case can be obtained by integrating with respect to M_{PBH} the top curves presented in Figures 7 to 16. In Table 1 we compile these global values for all the studied cases considering both simple collapse and critical collapse. We also determine in each case the contribution of Ω_{PBH} to the Cold Dark Matter density parameter $\Omega_{CDM} = 0.265$ (cf. Planck Collaboration et al., 2020).

The total value of the number of PBHs, N_{PBH}, can also be obtained by integrating with respect to M_{PBH} the curves at the bottom of Figures 7 to 16. In Table 2 we compile these total values for all the studied cases considering both simple collapse and critical collapse. We also determine the N_{PBH} maximum location, i.e., the mass for each of the curves. In Table 3 we show the mass spectra where PBH formation occurs for both regimes.

Table 1: The global value of the PBH density parameter Ω_{PBH} at the present time for all the studied scenarios under the simple collapse and critical collapse regimes. It is also shown the contribution of Ω_{PBH} to the Cold Dark Matter density parameter Ω_{CDM}.

			Simple collapse		Critical collapse	
$\log\left(\frac{t_k}{1\text{ s}}\right)$	n_{max}	QCD	Ω_{PBH}	$\frac{\Omega_{PBH}}{\Omega_{CDM}}(\%)$	Ω_{PBH}	$\frac{\Omega_{PBH}}{\Omega_{CDM}}(\%)$
-1	1.948	all	9.08×10^{-6}	3.43×10^{-3} %	1.53×10^{-6}	5.79×10^{-4} %
-3	1.808	CM	3.64×10^{-4}	0.137 %	6.09×10^{-5}	2.30×10^{-2} %
-5	1.708	CM	2.50×10^{-2}	9.45 %	4.40×10^{-3}	1.66 %
-7	1.619	CM	1.05×10^{-2}	3.96 %	1.75×10^{-3}	0.66 %
-9	1.553	CM	8.01×10^{-2}	30.2 %	1.32×10^{-2}	5.00 %

Table 2: The total number of PBHs at the present time within a volume of 1 Gpc^3 for all the studied scenarios under the simple collapse and critical collapse regimes. It is also shown the location, in solar masses, where the maximum of PBHs formation occurs.

			Simple collapse		Critical collapse	
$\log\left(\frac{t_k}{1\ \mathrm{s}}\right)$	n_{max}	QCD	$N_{PBH}^{total}(Gpc^{-3})$	Peak ($M_\odot$)	$N_{PBH}^{total}(Gpc^{-3})$	Peak ($M_\odot$)
-1	1.948	all	3.15×10^{11}	3.32×10^{3}	3.11×10^{11}	5.89×10^{2}
-3	1.808	CM	2.63×10^{15}	16.5	2.53×10^{15}	2.79
-5	1.708	CM	2.02×10^{19}	0.123	1.99×10^{19}	2.21×10^{-2}
				2.20		0.407
-7	1.619	CM	1.50×10^{21}	7.18×10^{-4}	1.48×10^{21}	1.23×10^{-4}
-9	1.553	CM	2.20×10^{24}	3.60×10^{-6}	2.17×10^{24}	6.03×10^{-7}

Table 3: The mass spectrum for which N_{PBH} per Gpc^3 at the present time is at least 1 for all the studied scenarios under the simple collapse and critical collapse regimes.

			Simple collapse	Critical collapse
$\log\left(\frac{t_k}{1\ \mathrm{s}}\right)$	n_{max}	QCD	$M_{PBH}(M_\odot)$	$M_{PBH}(M_\odot)$
-1	1.948	all	$[3.90 \times 10^{2} - 4.59 \times 10^{4}]$	$[0.135 - 9.44 \times 10^{3}]$
-3	1.808	CM	$[1.43 - 6.40 \times 10^{2}]$	$[1.43 \times 10^{-5} - 1.30 \times 10^{2}]$
-5	1.708	CM	$[4.64 \times 10^{-3} - 11.8]$	$[6.92 \times 10^{-9} - 2.63]$
-7	1.619	CM	$[1.81 \times 10^{-5} - 0.11]$	$[7.76 \times 10^{-12} - 2.09 \times 10^{-2}]$
-9	1.553	CM	$[4.97 \times 10^{-8} - 1.42 \times 10^{-3}]$	$[2.54 \times 10^{-15} - 2.60 \times 10^{-4}]$

In Figures 17 to 21 (top) the grey-shaded region represents the area where PBH formation occurs, i.e., where $N_{PBH}(t_0) \geq 1$ (cf. equation 31) for the critical collapse regime. The line on top of the grey-shaded region represents the same but now considering the simple collapse regime. In addition, it is also shown in Figures 17 to 21 (bottom) the PBH distribution at the present time in the form of a density plot. Both plots were obtained by using the matrix A_N.

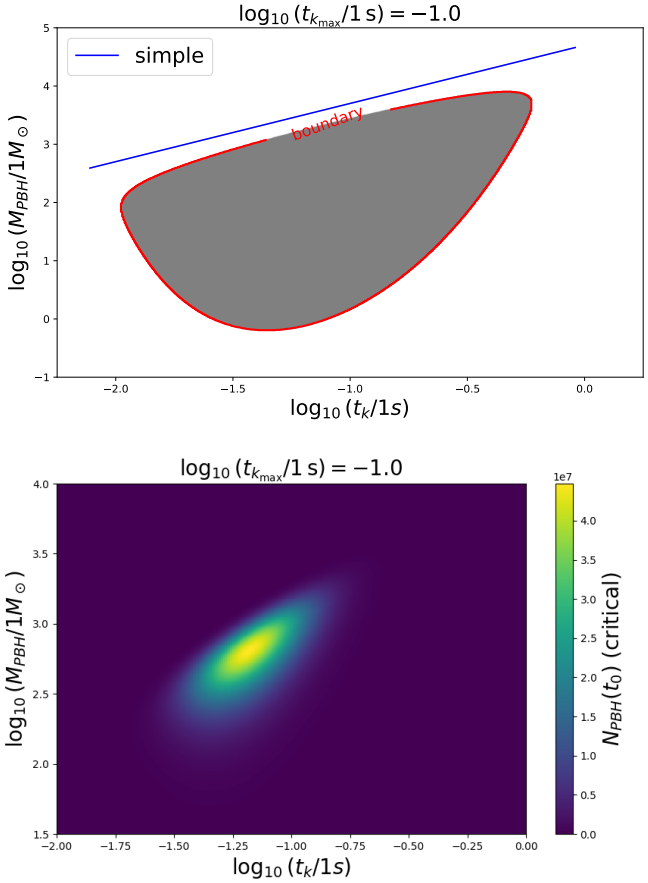

Figure 17: The plot containing the grey-shaded region satisfying the inequality $N_{PBH}(t_0) \geq 1$ (top) and the density plot (bellow) for $N_{PBH}(t_0)$ when $t_{k_{max}} = 10^{-1}$ s. In the top plot it is also shown the line representing the simple collapse regime (see text for more details).

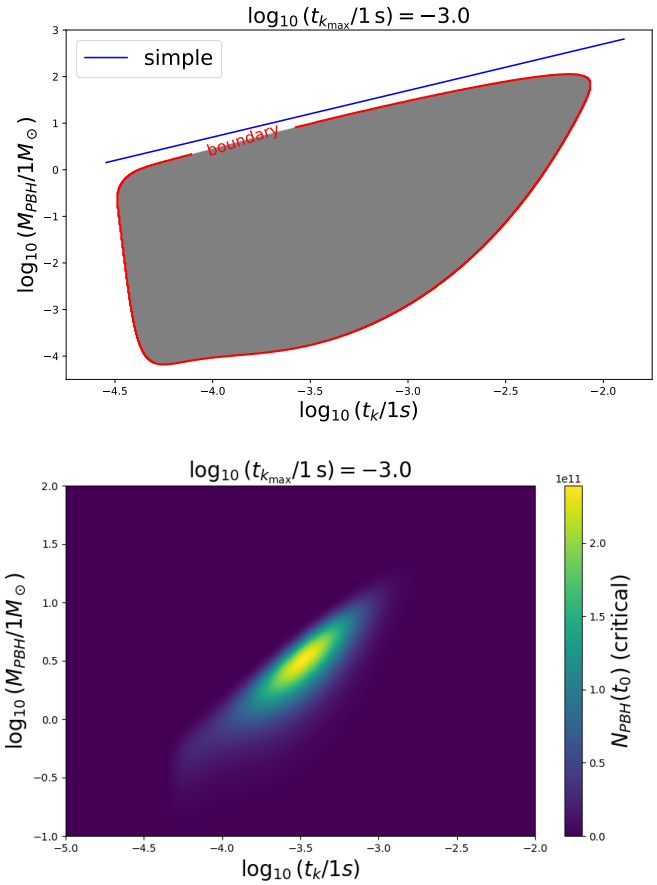

Figure 18: The plot containing the grey-shaded region satisfying the inequality $N_{PBH}(t_0) \geq 1$ (top) and the density plot (bellow) for $N_{PBH}(t_0)$ when $t_{k_{max}} = 10^{-3}$ s. In the top plot it is also shown the line representing the simple collapse regime (see text for more details).

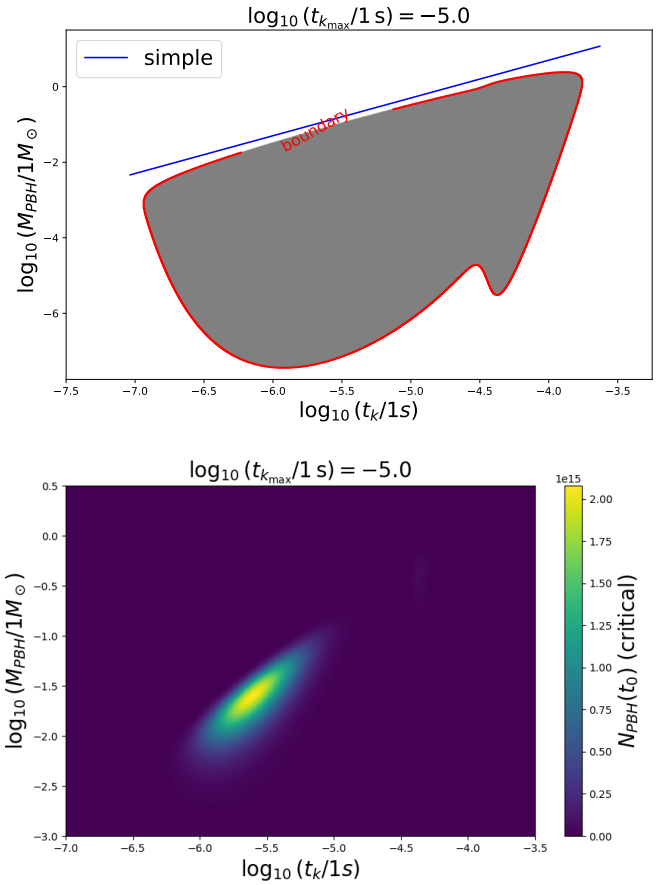

Figure 19: The plot containing the grey-shaded region satisfying the inequality $N_{PBH}(t_0) \geq 1$ (top) and the density plot (bellow) for $N_{PBH}(t_0)$ when $t_{k_{max}} = 10^{-5}$ s. In the top plot it is also shown the line representing the simple collapse regime (see text for more details).

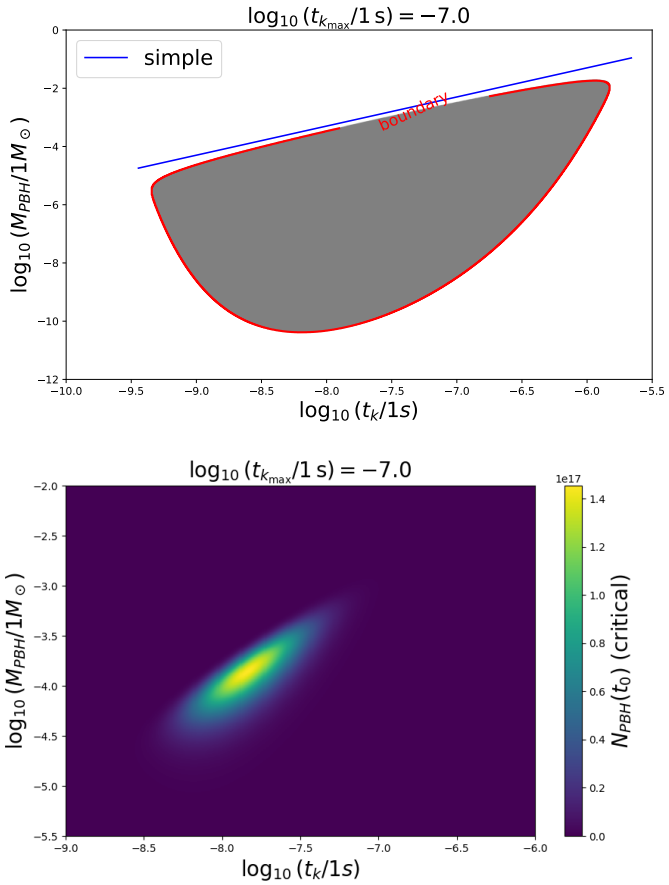

Figure 20: The plot containing the grey-shaded region satisfying the inequality $N_{PBH}(t_0) \geq 1$ (top) and the density plot (bellow) for $N_{PBH}(t_0)$ when $t_{k_{max}} = 10^{-7}$ s. In the top plot it is also shown the line representing the simple collapse regime (see text for more details).

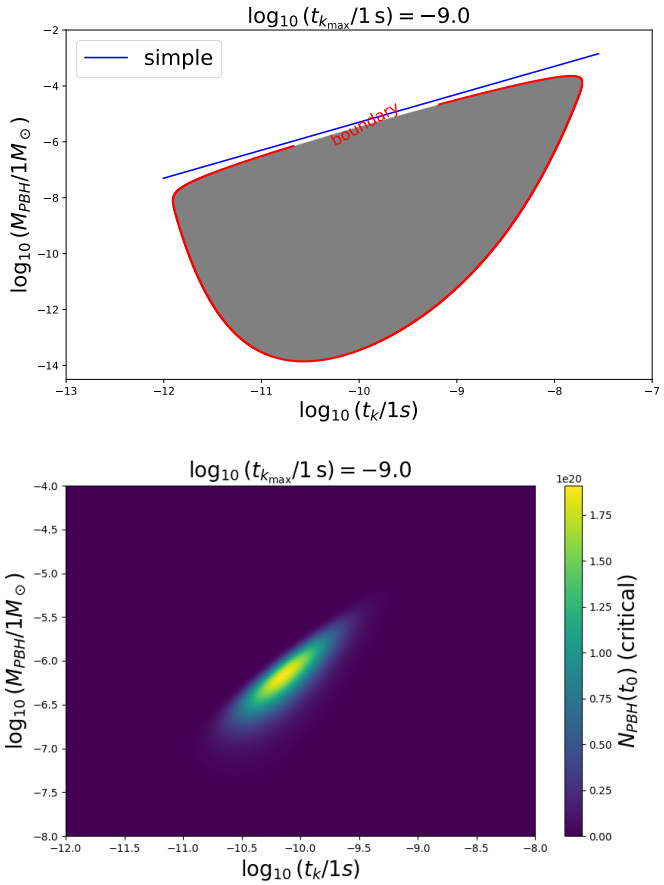

Figure 21: The plot containing the grey-shaded region satisfying the inequality $N_{PBH}(t_0) \geq 1$ (top) and the density plot (bellow) for $N_{PBH}(t_0)$ when $t_{k_{max}} = 10^{-9}$ s. In the top plot it is also shown the line representing the simple collapse regime (see text for more details).

4 Conclusions and future work

PBHs may have formed in the early Universe due to the collapse of density fluctuations, provided that the fluctuations exceed some threshold δ_c. During the radiation-dominated Universe the value of this threshold remains constant. However, if the Universe experiences some phase transition such as the QCD phase transition then we might have a decrease on the value of δ_c which in turn facilitates the formation of PBHs. In order to allow PBH formation at some scale k on the early Universe, the value of the spectrum index of the fluctuations $n(k)$ should have been blue (i.e., $n(k) > 1$) at least during some periods.

It is often assumed that the majority of the PBHs formed at a particular epoch would have masses within the order of the horizon mass (M_H) at that epoch. However, if critical gravitational collapse is taken into account, then we might have PBHs formation with a broader mass spectrum. We refer to the first situation as **simple collapse** in opposition to the latter that is known as **critical collapse**. We have explored the process of critical collapse for PBH formation during the QCD epoch in the framework of a CM.

We have considered five different cases: $t_{k_{max}} = 10^{-1}$ s, $t_{k_{max}} = 10^{-3}$ s, $t_{k_{max}} = 10^{-5}$ s, $t_{k_{max}} = 10^{-7}$ s, and $t_{k_{max}} = 10^{-9}$ s (with $t_{k_{max}}$ representing the instant for which $n(k)$ attains its maximum value). For each case, we have determined the curves giving the PBH density parameter (Ω_{PBH}) and the PBH number (N_{PBH}) per Gpc^3 for both the simple and critical collapse (Figures 7 to 16). We have also determined, for each of the five cases, the Ω_{PBH} and N_{PBH} global values evaluated at the present time (Tables 1 and 2). We notice that at earlier epochs PBHs formed in greater numbers but with smaller masses. As we move forward in time, the number of PBHs formed decreases, but their masses increase, for both the simple and critical regimes. In Table 1, besides the global value of Ω_{PBH}, it is also shown the contribution of this value to Ω_{CDM}. In Table 2 it is also shown the location, in solar masses, for the maximum value exhibited by the curve N_{PBH}.

Regarding the PBH density parameter $\Omega_{\rm PBH}$ it appears, in both regimes, that as we go along from $t_{\rm k} = 10^{-1}$ s to $t_{\rm k} = 10^{-9}$ s there is an increase in the value of Ω_{PBH} and therefore an increase on the contribution to the value of Ω_{CDM}, with the case $t_{\rm k} = 10^{-7}$ s being the exception (cf. Table 1). However, we must bear in mind that the cases studied correspond to situations in which we attempted to go as far as it was allowed by the observational constraints. The exception reported for the case $t_{\rm k} = 10^{-7}$ s is a direct consequence of the observational constraints (see Figures 2 to 6).

In Table 3 we show the PBH mass spectrum for all the studied scenarios and for both collapse regimes. In Figures 17 to 21 we show the region in the plane $(\log(t_k), \log(M_{PBH}))$ where PBH formation occurs within the critical collapse regime together with the line representing the simple collapse regime. Besides that, we show the value of N_{PBH} for each cell in the same plane in the form of a density plot.

From the analysis of Table 3 we see that under the critical collapse regime the mass spectrum is much broader. In the case of $t_{k_{max}} = 10^{-5}$ s, for example, the mass spectrum extends from $\sim 10^{-3}\ M_\odot$ up to $\approx 10\ M_\odot$ for the simple collapse regime and from $\sim 10^{-9}\ M_\odot$ up to $\approx 3\ M_\odot$ when the critical collapse regime is taken into account. Despite this difference in the extent of the mass spectrum, it can be seen that the value of N_{PBH}^{total} is of the same order for both regimes (cf. Table 2). In the case of $t_{k_{max}} = 10^{-5}$ s, for

example, we have $\sim 10^{19}$ PBHs per Gpc^3 regardless of the regime considered.

Although the number of PBHs is of the same order of magnitude in both regimes, though consistently slightly lower in the critical collapse regime (cf. Table 2), the same does not happen when we are talking about the contribution to the value of the Ω_{CDM} parameter with the critical collapse giving always lower contributions (cf. Table 1). In the case $t_{k_{max}} = 10^{-5}$ s, for example, we have a contribution of 1.66% under the critical collapse against 9.45% obtained when considering the simple collapse. This happens because, although we have practically the same number of PBHs for both regimes, in the critical collapse regime they are dispersed over a wider mass range with a propensity for lower masses (cf. Table 3).

In terms of future work we intend to extend our study regarding the formation of PBHs during the QCD epoch due to critical collapse to the Bag Model (BM) and Lattice Fit Model (LFM) as well. Beyond that, it would also be worth studying the effect of critical collapse for different epochs such as the Electroweak phase transition and the cosmological electron-positron annihilation epoch.

References

Blais D., Bringmann T., Kiefer C., Polarski D., 2003, *Accurate results for primordial black holes from spectra with a distinguished scale*, PhRvD, 67, 024024. doi:10.1103/PhysRevD.67.024024

Carr B. J., 1975, *The primordial black hole mass spectrum*, ApJ, 201, 1. doi:10.1086/153853

Carr B. J., 2003, *Primordial Black Holes as a Probe of Cosmology and High Energy Physics*, LNP, 631, 301. doi:10.1007/978-3-540-45230-0_7

Carr B., Kühnel F., Sandstad M., 2016, *Primordial black holes as dark matter*, PhRvD, 94, 083504. doi:10.1103/PhysRevD.94.083504

Carr B., Kohri K., Sendouda Y., Yokoyama J., 2021, *Constraints on Primordial Black Holes*, RPPh, 84, 116902. doi:10.1088/1361-6633/ac1e31

Erfani E., 2014, *Modulated inflation models and primordial black holes*, PhRvD, 89, 083511. doi:10.1103/PhysRevD.89.083511

Hawking S., 1971, *Gravitationally collapsed objects of very low mass*, MNRAS, 152, 75. doi:10.1093/mnras/152.1.75

Jesus P. D. F., Sobrinho J. L. G., June 2025, *A plotting on primordial black holes observational constraints*, Relatório do trabalho desenvolvido ao abrigo do programa INGRESSA 2025 da Secretaria Regional da Educação - Direção Regional de Juventude (92 pp.)

Kuhnel F., Rampf C., Sandstad M., 2015, *Effects of Critical Collapse on Primordial Black-Hole Mass Spectra*, arXiv, arXiv:1512.00488. doi:10.48550/arXiv.1512.00488

Musco I., De Luca V., Franciolini G., Riotto A., 2021, *Threshold for primordial black holes. II. A simple analytic prescription*, PhRvD, 103, 063538. doi:10.1103/PhysRevD.103.063538

Musco I., Jedamzik K., Young S., 2024, *Primordial black hole formation during the QCD phase transition: threshold, mass distribution and abundance*, PhRvD, 109, 083506. doi:10.1103/PhysRevD.109.083506

Musco I., Miller J. C., 2013, *Primordial black hole formation in the early universe: critical behaviour and self-similarity*, CQGra, 30, 145009. doi:10.1088/0264-9381/30/14/145009

Niemeyer J. C., Jedamzik K., 1998, *Near-Critical Gravitational Collapse and the Initial Mass Function of Primordial Black Holes*, PhRvL, 80, 5481. doi:10.1103/PhysRevLett.80.5481

Niemeyer J. C., Jedamzik K., 1999, *Dynamics of Primordial Black Hole Formation*, PhRvD, 59, 124013. doi:10.1103/PhysRevD.59.124013

Novikov I. D., Polnarev A. G., Starobinskii A. A., Zeldovich I. B., 1979, *Primordial black holes*, A&A, 80, 104

Planck Collaboration, Ade P. A. R., Aghanim N., Arnaud M., Arroja F., Ashdown M., Aumont J., et al., 2016, *Planck 2015 results. XX. Constraints on inflation*, A&A, 594, A20. doi:10.1051/0004-6361/201525898

Planck Collaboration, Aghanim N., Akrami Y., Ashdown M., Aumont J., Baccigalupi C., Ballardini M., et al., 2020, *Planck 2018 results. VI. Cosmological parameters*, A&A, 641, A6. doi:10.1051/0004-6361/201833910

Ricotti M., Ostriker J. P., Mack K. J., 2008, *Effect of Primordial Black Holes on the Cosmic Microwave Background and Cosmological Parameter Estimates*, ApJ, 680, 829. doi:10.1086/587831

Saglia R. P., Opitsch M., Erwin P., Thomas J., Beifiori A., Fabricius M., Mazzalay X., et al., 2016, *The SINFONI Black Hole Survey: The Black Hole Fundamental Plane Revisited and the Paths of (Co)evolution of Supermassive Black Holes and Bulges*, ApJ, 818, 47. doi:10.3847/0004-637X/818/1/47

Sobrinho J. L. G., 2011, *The possibility of primordial black hole direct detection*, PhD thesis., Univ. Madeira, Available at: `http://hdl.handle.net/10400.13/235`

Sobrinho J. L. G., Augusto P., Gonçalves A. L., 2016, *New thresholds for primordial black hole formation during the QCD phase transition*, MNRAS, 463, 2348. doi:10.1093/mnras/stw2138

Sobrinho J. L. G., Augusto P., 2007, *The fraction of the Universe going into Primordial Black Holes*, CCM Internal Report nr.126/07 (109 pp.)

Sobrinho J. L. G., Augusto P., 2014, *Direct detection of black holes via electromagnetic radiation*, MNRAS, 441, 2878. doi:10.1093/mnras/stu786

Sobrinho J. L. G., Augusto P., 2020, *Stellar mass Primordial Black Holes as Cold Dark Matter*, MNRAS, 496, 60. doi:10.1093/mnras/staa1437

Sobrinho J. L. G., Augusto P., 2024, *Primordial intermediate and supermassive black hole formation during the electron-positron annihilation epoch*, MNRAS, 531, L40. doi:10.1093/mnrasl/slae028